Astron. Astrophys. 339, 737–744 (1998)

ASTRONOMY AND ASTROPHYSICS

^{13}CO at the centre of M 82

N. Neininger[1,2,3], M. Guélin[3], U. Klein[1], S. García-Burillo[4], and R. Wielebinski[2]

[1] Radioastronomisches Institut der Universität Bonn, Auf dem Hügel 71, D-53121 Bonn, Germany
[2] Max–Planck–Institut für Radioastronomie, Auf dem Hügel 69, D-53121 Bonn, Germany
[3] Institut de Radioastronomie Millimétrique, 300 rue de la Piscine, F-38406 St. Martin d'Hères, France
[4] Observatorio Astronómico Nacional, Apartado 1143, E-28800 Alcalá de Henares, Spain

Received 14 August 1997 / Accepted 1 September 1998

Abstract. Using the IRAM interferometer, we have observed the nearby starburst galaxy M 82 with a $4\farcs2$ resolution ($\simeq$ 70 pc) in the 1→0 line of ^{13}CO and in the λ 2.6-mm continuum.

The spatial distribution of the ^{13}CO line shows the same gross features as the ^{12}CO(1→0) map of Shen & Lo (1995), namely two lobes and a compact central source, though with different relative intensities. The lobes are more conspicuous and the central source is fainter in ^{13}CO than in ^{12}CO.

The velocity field observed around the nucleus shows a very steep gradient (140 km s^{-1} over 75 pc), which is very probably caused by the stellar bar visible in the near infrared. The dynamical centre coincides with the IR peak and is shifted $6''$ north-east of the compact ^{13}CO source. The two CO lobes appear to be associated with the ends of the bar and not with a molecular ring, as usually assumed. They are probably shaped by the strong UV radiation from the central region. ^{13}CO must be more photodissociated than the self-shielded ^{12}CO molecules in the central ∼250 pc region, which may explain the relative weakness of the ^{13}CO central source.

A 130 pc-wide bubble of molecular gas has been identified, which happens to host the most luminous compact radio source in M 82. It lies 120 pc west of the IR peak between the central source and the western lobe and seems characterized by warmer gas, strong UV radio free-free radiation, and an enhanced cosmic ray production rate.

Key words: ISM: bubbles – galaxies: individual: M 82 – galaxies: ISM – galaxies: kinematics and dynamics – galaxies: starburst – radio lines: galaxies

1. Introduction

The central kpc region of M 82, the archetype of starburst galaxies, provides a unique laboratory to study intense star formation from an assembly of giant molecular clouds. The starburst, possibly triggered by a tidal interaction with M 81, manifests itself through a high far-infrared (far IR) luminosity and a high density of supernova remnants (SNR) (see e.g. Telesco & Harper 1980; Kronberg et al. 1985). The presence of copious molecular gas is obvious from the many single-dish studies of the CO mm lines (Nakai et al. 1987; Olofsson & Rydbeck 1984; Loiseau et al. 1988, 1990). A large fraction of this gas is concentrated in massive hot and dense clouds, which give rise to conspicuous emission in dozens of high-excitation molecular lines, such as the high-J lines of CO and the lines of CS and HCN (Henkel & Bally 1985, Wild et al. 1992). These clouds, according to multi-transition analysis, have temperatures of ∼40 K and densities of few 10^4 cm^{-3} (Wild et al. 1992; Güsten et al. 1993). Interferometric observations show that they have a patchy distribution (Lo et al. 1987; Brouillet & Schilke 1993; Shen & Lo 1995).

The molecular gas at the centre of M 82 is usually thought to be concentrated in a rotating circumnuclear torus (e.g. Nakai et al. 1987, Shen & Lo 1995). The presence of a stellar bar (Telesco & Gezari 1992) may explain how gas is driven inwards in order to fuel the starburst. The main activity is however already subsiding according to Rieke et al. (1993, see also Shen & Lo 1995); this may seem surprising given the large amount of molecular gas in the "ring".

Multi-transition analysis show that the ^{12}CO mm lines are optically thick in M 82 (Wild et al. 1992), which makes it hazardous to study the gas distribution and kinematics of this edge-on galaxy from this isotopomer alone. The HI line, moreover, gives little insight into the kinematics of the central regions as its profile shows a mixture of emission and absorption components.

M 82 has been mapped in the optically thin ^{13}CO and C^{18}O lines (Loiseau et al. 1988, 1990; Wild et al. 1992), but with spatial resolutions of at best 150 pc. Both the ^{13}CO brightness distribution and velocity field appeared markedly different from those observed in ^{12}CO, an unusual result at such low resolutions. Single-dish studies of compact and weak extragalactic sources, however, are hampered by insufficient resolution and pointing errors. An interferometric study in the optically thin ^{13}CO line was therefore mandatory. Here we present such a study carried out with the IRAM Plateau de Bure interferometer. In Sect. 2 we describe the observations and data analysis. Sect. 3 presents the distribution and kinematics of the ^{13}CO emission. A prominent molecular arc-structure is described and dicussed in Sect. 4. Sect. 5 analyzes the observations in the frames of the circumnuclear torus and bar scenarios. Finally, we give our conclusions in Sect. 6.

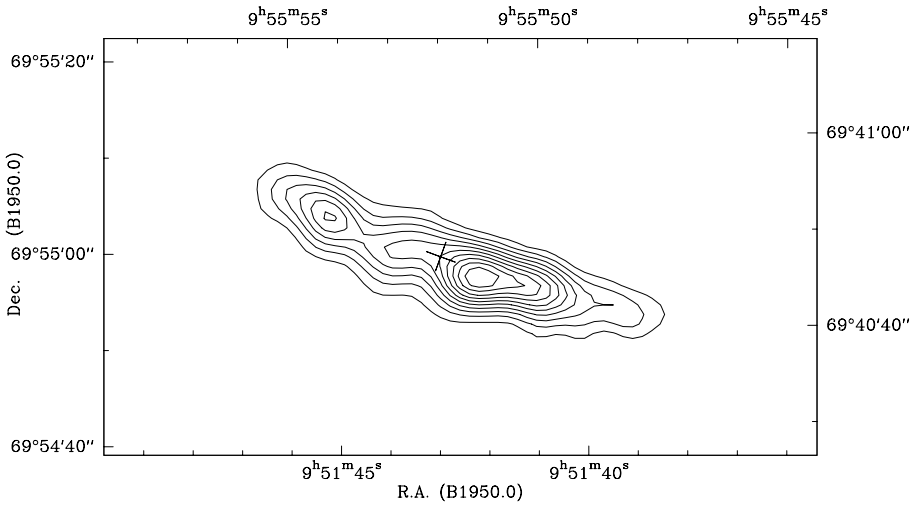

Fig. 1. Map of the continuum emission of M 82 at 2.7 mm. The contour interval is 5 mJy/beam (0.03 K). The cross marks the position of the $\lambda 2.2$ μm nucleus derived by Joy et al. (1987). Note that in this figure the J2000.0 coordinates are given for comparison at the upper and right sides of the box. The field of view is identical to those of Figs. 2, 3 and 4.

2. Observations and data reduction

The central region of M 82 was observed in the 1→0 line of ^{13}CO ($\nu_{\rm obs}$ = 110.116824 GHz) with the IRAM interferometer at Plateau de Bure. The surveyed area is centred on the 2.2μm nucleus (at $\alpha = 09^h51^m43\overset{s}{.}4, \delta = 69°55'00''$ B1950.0), Joy et al. (1987); see also Lester et al. (1990) and consists of three overlapping fields corresponding to three pointings of the $45''$ FWHM primary beam, shifted, respectively, by (α, δ)=$(-20'', -9'')$, $(0'', 0'')$, and $(+20'', +9'')$ with respect to the nucleus. These fields were successively observed for 6 minutes each, the observing sequence being completed by a 4 min. integration on a phase calibrator (0716+714). We used the 'compact' CD antenna configuration, with a longest baseline of 176 m and a shortest one of 24 m. The six units of the correlator were combined to cover a 1500 km s^{-1}-wide band, with a velocity resolution of 6.4 km s^{-1} and a 40 km s^{-1}-wide band centred on the source systemic velocity, $V_{sys}(LSR) = 225$ kms^{-1}, with a 0.4 km s^{-1} resolution. The continuum level was derived in the lower sideband of the receiver (110 GHz) from the outer channels ($|V(LSR) - V_{sys}(LSR)| \geq 200$ kms^{-1}) of the broad band and in the upper sideband (113 GHz) from the entire 1500 km s^{-1}-wide band.

The observations were carried out in August 1994 (4 antennas, D configuration) and October 1994 (3 antennas, C1+C2 configurations); the D configuration observations were repeated in April 1995 (4 antennas). For the calibration of the data we used 0923+392, 3C84, 3C345 and 3C454.3 as primary amplitude and RF bandpass calibrators. In the data reduction process, the transfer function was tapered with a 90-m (FWHP) Gaussian to yield a circular synthesized beam of size $4\overset{''}{.}2$, which at the adopted distance of M 82 (3.25 Mpc) corresponds to 66 pc. The 3 fields were combined as a mosaic and subsequently cleaned using the MAPPING procedure of the GILDAS package; this yields a roughly constant sensitivity along the line joining the centres of the 3 fields.

3. Results

3.1. Continuum emission at 110 GHz

Fig. 1 shows the continuum map constructed from the line emission-free channels of the upper (113 GHz) and lower (110 GHz) receiver sidebands. The average wavelength is close to 2.7 mm. The rms noise in this map is 2.5 mJy/beam (14 mK), its resolution $4\overset{''}{.}2$. Comparison with the continuum maps of Carlstrom & Kronberg (1991), Brouillet & Schilke (1993) and Seaquist et al. (1996) shows a tight correspondence between all the four interferometric maps in the range 90–110 GHz.

The mm continuum emission in M 82 is a mixture of thermal free-free, nonthermal synchrotron, and thermal dust emissions (Klein et al. 1988). Free-free emission is expected to dominate largely at λ 3 mm, the relativistic electrons having lost too much energy to radiate significantly at this short wavelength; therefore, one expects a nearly flat spectrum (see Carlstrom & Kronberg 1991). Integrating the flux density over our 110 GHz map, we derive a value of 0.55 ± 0.05 Jy, in good agreement with the values measured at lower frequencies by other groups (Jura et al. 1978; Carlstrom & Kronberg 1991; Brouillet & Schilke 1993; Seaquist et al. 1996). This confirms the thermal free-free nature of the continuum radiation.

3.2. ^{13}CO line emission

In Fig. 2 we show the CLEANed velocity-channel maps[1] between $+128$ km s^{-1} and -179 km s^{-1}. The velocity resolution has been degraded to 12.8 km s^{-1} for the sake of clarity. These channel maps cover the velocity range within which strong ^{13}CO emission was found. Significant emission was actually detected over a larger velocity range (+140 km s^{-1} to -190 km s^{-1}). Positive velocity-channels are dominated by an emission "lobe", centred $\simeq 15''$E of the nucleus. This lobe stays at about the same place from +130 to $+60$ km s^{-1}, while its position angle turns from $\sim 70°$ to $\sim 45°$. Near +100 km s^{-1}, a spur is seen to emerge to the N of the lobe. Between -64 km s^{-1}

[1] Unless specified otherwise, all velocities quoted in this paper are relative to the systemic velocity $V_{sys}(LSR) = +225$ km s^{-1}.

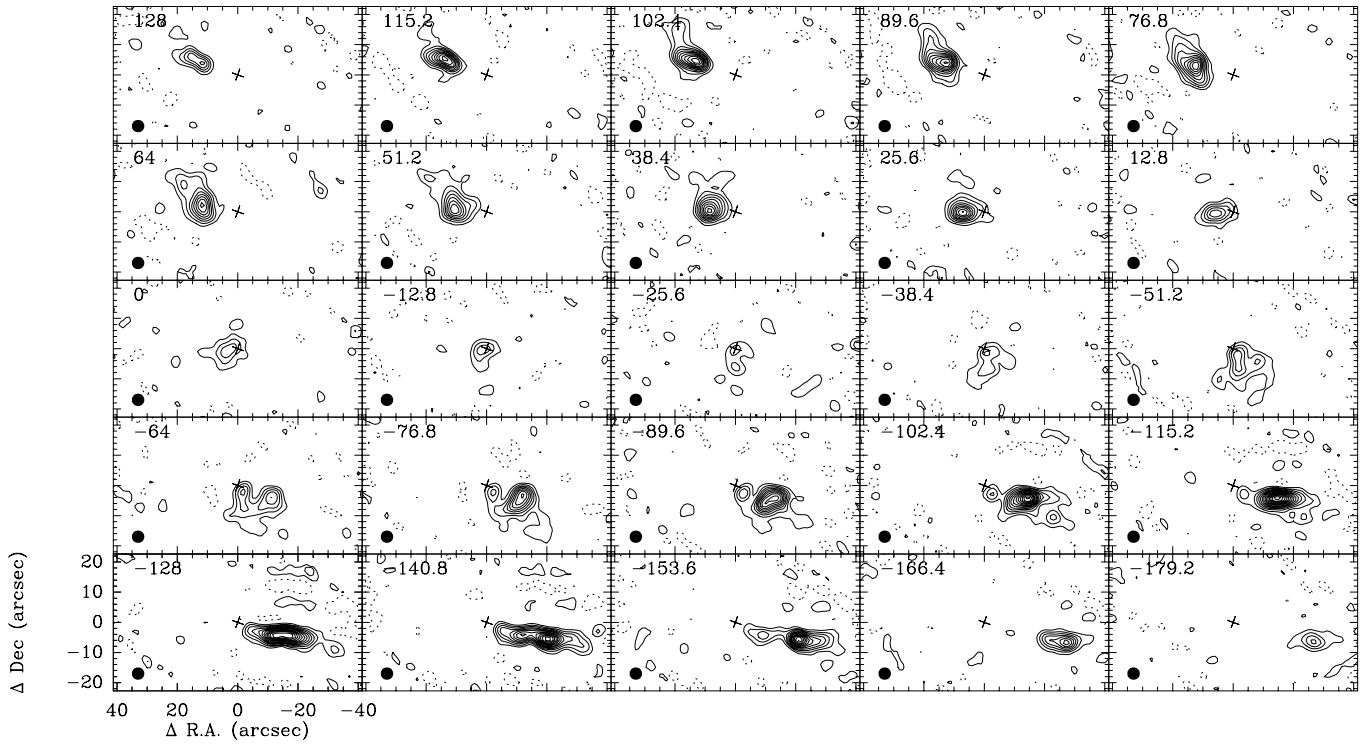

Fig. 2. ^{13}CO(1→0) velocity-channel maps. The offsets in R.A. and Dec are relative to the $\lambda 2$ μm nucleus which is denoted by a cross (R.A. $09^h51^m43\overset{s}{.}4$, Dec $69°55'00\overset{''}{.}0$ B1950.0, Joy et al. 1987); E is left, N up. Each velocity-channel is 12.8 km s^{-1} wide; its centre velocity is indicated in the top left corner in units of km s^{-1}. Velocity 0 corresponds to the galaxy systemic velocity, $V_{sys}(LSR) = +225$ km s^{-1}. The intensities are corrected for attenuation by the primary beam. The first contour level and the contour interval are 20 mJy/beam (0.1 K). The black dot in the bottom left corner of each map represents the half-power synthesized beam.

and -90 km s^{-1} an arc-like structure is clearly visible. The negative velocity-channels are however dominated by a second emission lobe, W of the nucleus. It extends further out and to larger velocities than the eastern lobe; its orientation is almost E-W. Emission is also detected within 5″ of the nucleus. It extends from $+26$ km s^{-1} to -154 km s^{-1}, a remarkably large velocity range.

Fig. 3 shows the ^{13}CO(1→0) velocity-integrated line intensity (zeroth moment of the data cube). Its distribution differs markedly from the continuum emission distribution of Fig. 1. The two emission lobes appear much broader and conspicuous than in the continuum emission, and the "central" source ($\alpha = 09^h51^m42\overset{s}{.}3$, $\delta = 69°54'57\overset{''}{.}4$, B1950.0), much fainter. Note that the map is corrected for attenuation by the antenna primary beam and that its noise increases towards its edges. The reality of the weak features near $\alpha = 09^h51^m36^s$, at the western edge, is thus questionable (see also Sect. 3.3).

A comparison with the ^{12}CO(1→0) map of Shen & Lo (1995) shows good agreement of the most salient structures (see Fig. 4). There is an almost perfect spatial coincidence between the bright lobes in ^{13}CO and ^{12}CO which holds as well for the central peak, although this latter appears relatively brighter in ^{12}CO than in ^{13}CO. The faint outer extensions of the lobes in Figs. 2 and 3 are also present in ^{12}CO. The weak ^{13}CO extension, south of the nucleus near $\alpha = 09^h51^m43\overset{s}{.}0$, $\delta = 69°54'52\overset{''}{.}9$, has a counterpart in ^{12}CO; this structure seems to be made up by emission at ~ -50 km s^{-1} (see Fig. 2). Except for the stronger central source, the only marked difference between ^{12}CO and ^{13}CO is the absence of ^{13}CO emission to the N, at $\delta \sim 69°55'20''$. As a consequence, the $R =^{12}$CO/^{13}CO (1→0) line intensity ratio is about constant over most of the map and is close to 10, a value marginally larger than those observed in the bright nearby galaxies ($R = 7 - 10$, see e.g. García-Burillo et al. 1993). This ratio increases to $R =\simeq 20$ near the central CO source (C 1 in Shen & Lo's map), and could be even larger in the northern ^{12}CO source. The minor differences between the ^{13}CO and ^{12}CO maps seem hardly compatible with the large ones reported by Loiseau et al. (1990). It has to be noted, however, that their analysis is based on (2→1) data so that a direct comparison is not possible.

Comparing our ^{13}CO(1→0) with the HCN(1→0) map of Brouillet & Schilke (1993) we find an overall resemblance of the large-scale distribution, but also significant differences. Mainly, the central source is much more pronounced in all velocity channels in HCN than in ^{13}CO; conversely the lobes appear dimmer. The faint 50 kms^{-1} extension south of the nucleus and the arc-like structure 7″ west of the nucleus, discussed in the next section, are also discernable, though less clearly.

The ^{13}CO data cast doubts on the standard picture of a circumnuclear molecular torus. Firstly, the emission in Fig. 3 is strongly asymmetric with respect to the major and minor axes. Secondly, an edge-on torus should appear quite differently in the

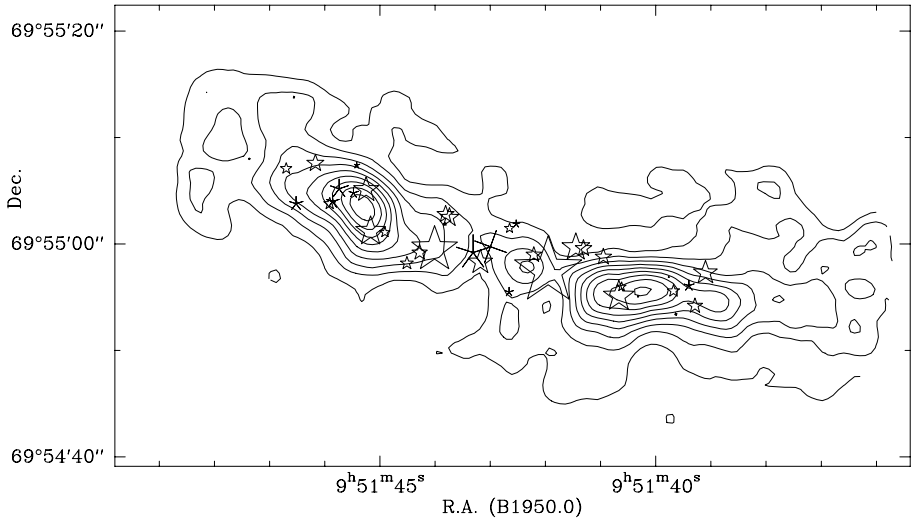

Fig. 3. Map of the integrated ^{13}CO(1→0) emission of M 82. Contour levels are 4, 6, 8... Jy/beam·km s^{-1}. The cross marks the position of the $\lambda 2$ μm nucleus as in Fig. 2. The radio SNR found by Kronberg et al. (1985) are indicated by stars whose sizes are proportional to the logarithm of the source flux densities; the SNR showing indications of free-free absorption (Wills et al. 1997) are denoted by open stars.

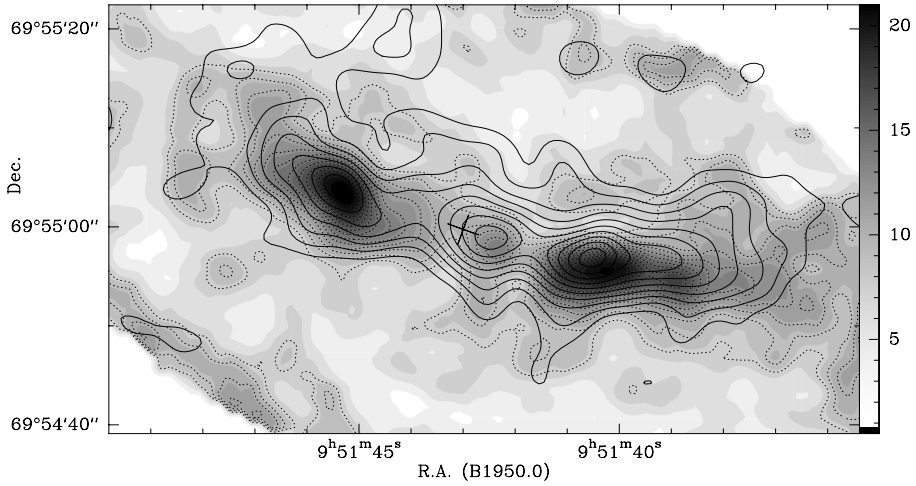

Fig. 4. Shen & Lo's ^{12}CO velocity-integrated contours smoothed to 3.″5, superimposed on a grey-scale map of the ^{13}CO integrated emission. First contour and contour interval are 25 Jy/beam·km s^{-1}; the ^{13}CO intensity code is indicated by the right scale and wedge (in Jy/beam·km s^{-1}). Note that due to the relatively small size of the IRAM primary beam, the ^{13}CO map becomes noisy at distances $> 30''$ from the major axis.

optically thin ^{13}CO line and in the optically thick ^{12}CO line. The ^{13}CO(1→0) line, for which $\tau \sim 0.1$ (Wild et al. 1992), should exhibit limb-brightening, i.e. two distant lobes, whereas the optically thick ^{12}CO line ($\tau \sim 7$) should show a more uniform distribution, and emphasize the near side of the torus. Instead, we observe remarkably similar distributions, which suggests that the CO is mostly concentrated in two or three sources.

The observations seem better interpreted in terms of molecular gas condensations located at the ends and in the middle of a stellar bar. Such condensations or "armlets" have already been observed in several galaxies, including NGC 1530 (Reynaud & Downes 1998) and NGC 891 (García-Burillo & Guélin 1995); Achtermann & Lacy (1995) and Larkin et al. (1994) have already proposed a similar model in order to explain the optical forbidden lines at the centre of M 82. We will see in the next sections that the kinematical data support this interpretation.

3.3. Kinematics of the ^{13}CO gas

Fig. 5 shows the velocity field derived from ^{13}CO(1→0) (first order moment), superimposed on the integrated intensity map. The dominant rotation pattern shows the eastern side receding (red-shifted) and the western side approaching (blue-shifted). There is a strong velocity gradient around the dynamical centre (offset (0,0) in Fig. 5), and the iso-velocity contours are systematically tilted by $\sim 30°$ with respect to the minor axis. This tilt is visible along the whole major axis of M 82, suggesting that the gas flow is driven by a non-axisymmetrical potential within the inner 500 pc. On the other hand, the velocity field is rather asymmetric, possibly due to the tidal interaction with M 81. A detailed analysis of individual features is thus difficult – even the inclination of the disk to the line of sight is hard to determine; analyses of the outer disk and the outflow cones suggest a value of $i \sim 80°$ (Götz et al. 1990).

The position angle (*PA*) of the major axis is slightly varying depending on the tracer and method used. That of the optical disk is usually given as $65°$, but Götz et al. (1990) used $60°$ for their thorough kinematical analysis of the optical emission lines. Other angles are also used, e.g. Achtermann & Lacy (1995) use $70°$ in the analysis of their NeII data. We re-determined the position of the kinematical major axis of the molecular gas from our data cube together with the position of the dynamical centre (see Fig. 5). The *PA* of this axis is $75°$, $10°$ different from that of the outer disk. The dynamical centre is found to coincide with the $\lambda 2\,\mu$m nucleus ($\alpha = 09^h51^m43\overset{s}{.}4$, $\delta = 69°55'00\overset{''}{.}0$ B1950.0, Joy et al. 1987).

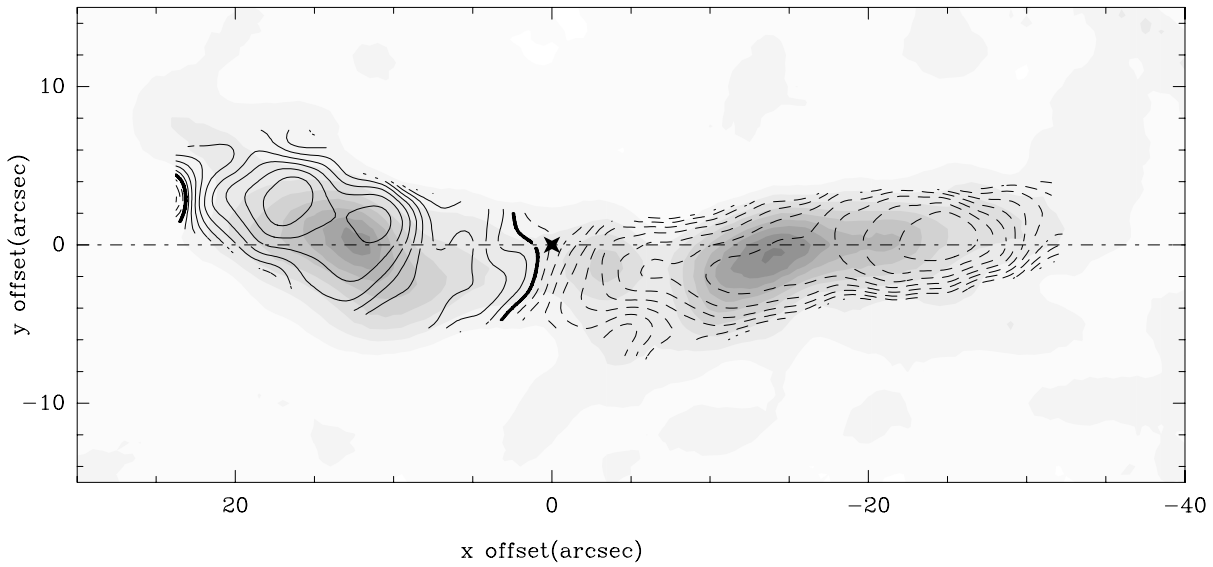

Fig. 5. Isovelocity contour levels, obtained from the first moment of ^{13}CO(1→0), overlaid on the integrated intensity map of Fig. 3 (grey scale). The thick line denotes $v = 0$ (or $V_{sys}(LSR) = +225$ km s^{-1}) and the level step is 10 kms^{-1}. Dashed contours indicate blue-shifted gas and full line contours red-shifted gas. x represents the offset along the galaxy major axis (point-dashed line, *PA* $= 75^{\circ}$) and y the offsets along the minor axis. x is positive towards the E-NE and y towards the the N-NW. The dynamical centre is indicated by a filled cross.

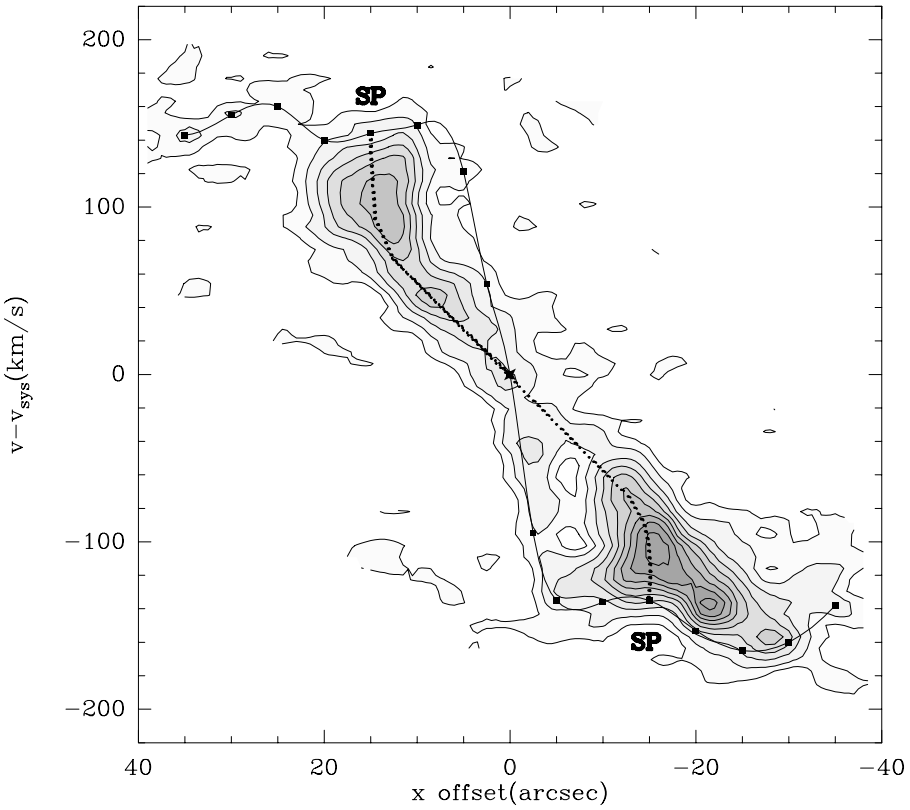

Fig. 6. Position-velocity diagramme taken along the major axis (grey scale and line contours from 10 to 300 mJy beam^{-1} by steps of 35 mJy beam^{-1}). The S-shaped pattern denoted as **SP** (dotted curve) locates the signature of the gaseous spiral arm response to the stellar bar. The terminal velocities along the major axis (square markers connected by a line) serve to derive v$_{rot}$.

Fig. 6 shows the position-velocity (p-v) diagramme taken along the major axis ($PA = 75^{\circ}$). Emission can be traced from -190 km s^{-1} to $+130$ km s^{-1}. This implies a rotation speed – *if this reflects simple rotation* – of $165/\sin(i)$ km s^{-1}, exactly the same figure as derived by Shen & Lo (1995). We would then obtain the same indicative mass for the central ~ 800 pc region of M 82 as Shen & Lo (7×10^8 M$_{\odot}$).

Although the ^{13}CO brightness distribution is very asymmetric, the main pattern of the p-v diagramme and the ridge of terminal frequencies are rather symmetric with respect to the dynamical centre. We note that emission from gas at high velocities is detected on both sides of the nucleus, although with a higher intensity for $x < 0$. The rotation curve derived from the terminal-velocities method applied to p-v diagramme

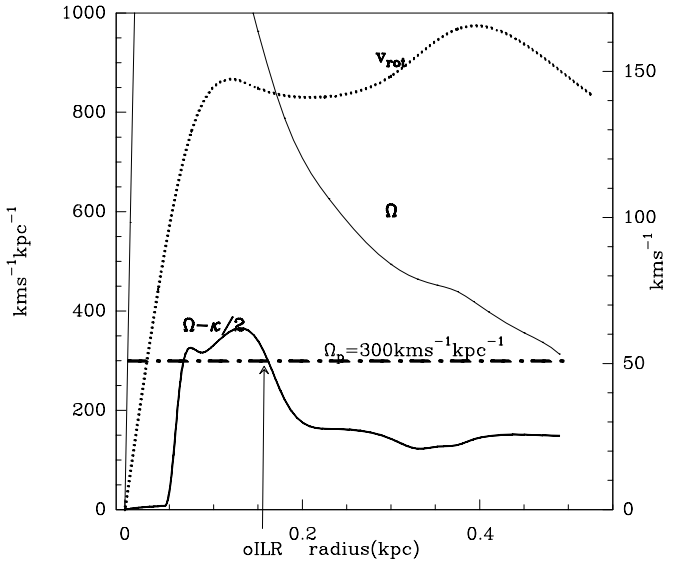

Fig. 7. Plot of the rotational velocity v_{rot}, of the angular frequency Ω, and of $\Omega - \kappa/2$, the angular minus the epicyclic frequency, for the inner 500 pc of M 82. For the assumed bar pattern speed of $\Omega_p = 300\,\mathrm{km s^{-1}\,kpc^{-1}}$, the oILR is at $r \sim 150$ pc.

is very steep: we estimate $v_{rot} \sim 140\,\mathrm{km\,s^{-1}}$ at $r \sim 75$ pc. From $r = 75$ pc to $r = 300$ pc the estimated rotation curve stays flat ($v_{rot} = 140\,\mathrm{km\,s^{-1}}$) and reaches a relative maximum of $v_{rot} = 160\,\mathrm{km\,s^{-1}}$ at $r = 375$ pc. The rotation curve (v_{rot}) and the related principal frequencies derived in the epicyclic approximation (Ω and Ω-κ/2) are represented in Fig. 7 for the inner 500 pc.

A large amount of gas is detected at velocities lower than determined by the ridge of terminal velocities shown in Fig. 6. There is an S-shaped feature in the p-v diagramme going across the dynamical centre (denoted as SP in Fig. 6). The characteristic pattern of SP suggests the presence of a non-axisymmetric distribution of molecular gas in the form of nuclear mini-spiral arms, which extend from the centre to $r \sim 300$ pc. Moreover, the 'figure-eight' pattern of the p-v diagramme formed by SP and the curve of terminal velocities is typical of a bar-driven gas flow (Kuijken & Merrifield 1995). The existence of a nuclear stellar bar of 1 kpc diameter was already established by Telesco & Gezari (1992), based on near-infrared observations in the J, K and I bands. Driven by a bar potential, gas clouds follow non self-intersecting ellipsoidal orbits. The major axes of these orbits precess as a function of radius, and hence end up delineating spiral arms, owing to orbit crowding. The precession of gas orbits is due to the dissipative nature of gas: molecular cloud-cloud collisions and the implied viscosity of the process cause a smooth transition between the bar-driven x_1 orbits (parallel to the bar major axis) towards x_2 orbits (perpendicular to bar major axis), when we go across the Inner Lindblad Resonance (ILR). Therefore, the presence of a nuclear bar potential and a spiral gas response are intimately related.

The existence of two ILRs in the nucleus of M 82 is clearly suggested by our observations (see Fig. 7). The ring-like appearance of the integrated intensity map (referred to in the literature as the molecular gas torus) indicates gas accumulation towards the outer ILR (oILR) at $r \sim 150$ pc caused by the action of gravitational torques by the stellar bar on the gas. If we assume that corotation of the stellar bar is located near its end-points ($r \sim 500$ pc), we derive a bar pattern speed of $\Omega_p = 300\,\mathrm{km s^{-1}\,kpc^{-1}}$ and from it, the location of two ILRs at r(iILR)$\sim$ 50 . . . 100 pc and r(oILR)$\sim$ 150 . . . 200 pc (see Fig. 7). The onset of a fast bar instability in the nucleus of M 82 is hardly surprising in view of the measured high values of $\Omega - \kappa/2$ within the inner 500 pc. Results of recent near-infrared surveys of galactic centres show that nuclear bar instabilities are ubiquitous and that the pattern speeds of these m=2 instabilities can reach high values on the derived kinematical major axis (see the case of M 100: García-Burillo et al. 1998). The final output would be the formation of a two-arm gaseous trailing spiral across the oILR. The tilting of isovelocity contours towards the centre, the ring-like concentration of molecular gas and the 'figure-eight' pattern of the major axis p-v plot support this theoretical scenario for the nucleus of M 82.

The steep negative-velocity feature between $x = 0$ and $x = -5''$, which is linked to the bar, was also observed in HCN(1→0) by Brouillet & Schilke (1993) and in ^{12}CO (1→0) by Shen & Lo (1995). It is more pronounced in HCN than in ^{12}CO or ^{13}CO, which probably denotes that the gas near the centre of the bar is dense.

4. A giant bubble

This steep negative-velocity feature merges into the western lobe at $-12''$, leaving a prominent hole in the p-v diagramme at $x = -7''$, v $= -50$ to $-100\,\mathrm{kms^{-1}}$. This "hole" is also visible in the velocity-channel maps of Fig. 2, where it appears as a $5''$-wide gap between the western lobe and the central source and centred at $\Delta\alpha = 7'', \Delta\delta = -2''$.

Fig. 8 shows a close-up view of velocity-channel maps around this hole. A faint arc-like structure (diameter $\sim 8''$, or 130 pc) delineates the southern border of the hole, while only very weak emission is visible to the north (at -51 km s^{-1}). The hole happens to host the young SNR 41.9+58 which is the strongest compact radio source in M 82 (Kronberg et al. 1985). This SNR is however assumed to be only about 40 years old (Wilkinson & de Bruyn 1990) and hence cannot be the origin of such a large structure. We note that the arc-like structure and the hole are also visible in the ^{12}CO velocity-channel maps shown by Lo et al. (1987) (e.g. in their map at $V_{\mathrm{LSR}} = 172$ km s^{-1}, which corresponds to $v = -53$ km s^{-1}).

The gas in the CO hole seems largely ionized. The H41α (Seaquist et al. 1985) and H110α (Seaquist et al. 1996) recombination line emissions show both a maximum, and the $4'' \times 7''$ wide associated HII region fills the hole in our ^{13}CO channel maps. The 3 mm continuum emission, which is essentially thermal free-free radiation, also peaks at this position. As concerns molecular lines, Wild et al. (1992) reported emission of high-J lines of HCO$^+$ and HCN from the region of the arc+hole, while lower excitation lines are less pronounced. The maximum of the atomic CI line falls close to this location (White et al. 1994).

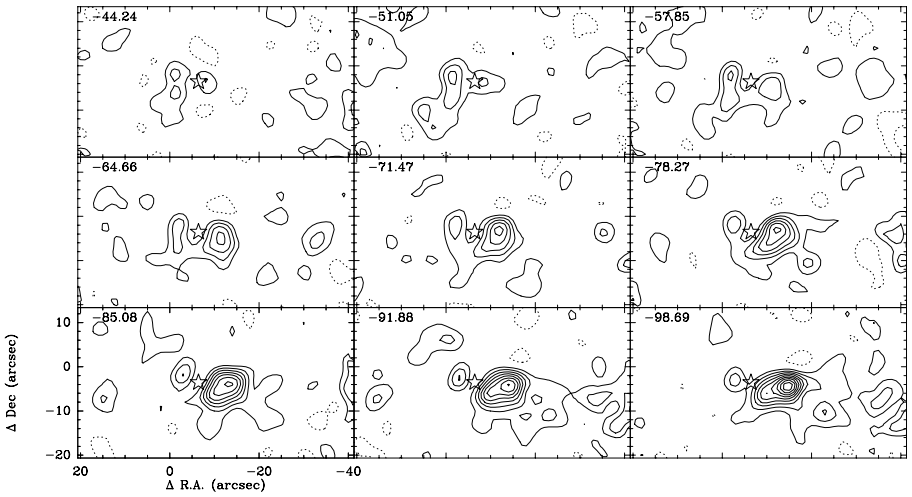

Fig. 8. Channel maps between -44 km s^{-1} and -99 km s^{-1}, centred on the emission hole and the arc-like feature. The star markes the position of the brightest compact continuum source in M 82, 41.9+58, located at $\alpha = 09^h51^m42\overset{s}{.}0$, $\delta = 69°54'57\overset{s}{.}4$.

Those authors also argued that the enhanced CI abundance in the central region of M 82 can be connected to a higher cosmic ray flux there. Copious cosmic rays could be delivered e.g. by the luminous compact source 41.9+58. Furthermore, as noted by Wild et al. (1992), the secondary peak in the 2.2μm image as well as the FIR and submm dust emission peaks (Joy et al. 1987; Smith et al. 1990) are found right there, and the maxima of the [NeII] line (Achtermann & Lacy 1995) are both close to this position. Finally, a recent high-resolution map at 408 MHz (Wills et al. 1997) clearly shows an emission-free circle of 100 pc diameter, right around this source, which is ascribed to a large photoionized zone. A realistic interpretation is that this is a region with an intense radiation field in which the atomic hydrogen has been ionized (see Wills et al. 1997). Such a region might have been created by a large cluster of massive stars whose stellar winds and supernova explosions (of which 41.9+58 is just the latest) can easily clear a large hole in the interstellar matter. Therein hot gas will be the dominant constituent and the intense radiation of the remaining stars will dissociate molecules unless they are shielded within dense clouds. This is consistent with the finding that the gas deficiency is less pronounced here in the HCN line (Sect. 3.2).

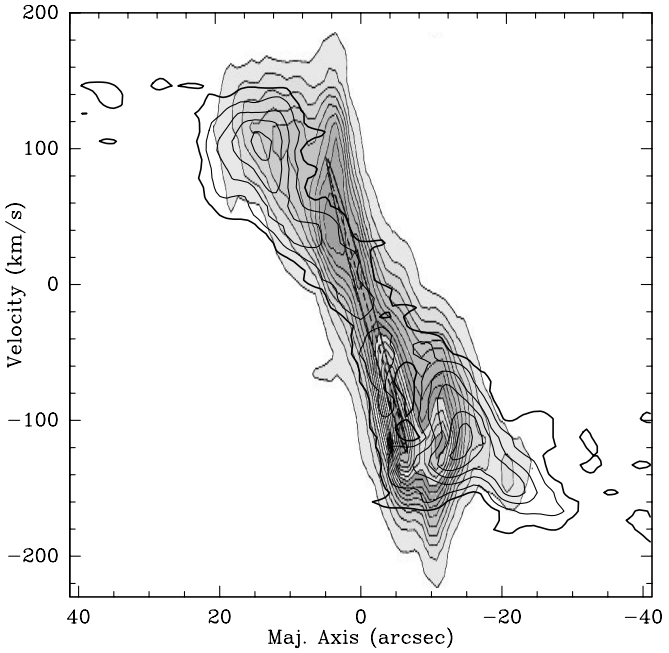

Fig. 9. Position-velocity diagramme of the [NeII] emission (adapted from Achtermann & Lacy 1995 – dense, shaded contours), superimposed onto that of the ^{13}CO(1→0) emission (thicker, widely spaced contours), and centred on $\alpha = 09^h51^m43\overset{s}{.}4$, $\delta = 69°55'00\overset{''}{.}0$, with position angle +70°. The [NeII] 'ring' as traced by the narrow ellipse has its endpoints in regions void of ^{13}CO emission.

5. The fueling of the starburst

In order to try to understand the remarkable morphology and kinematics of the central 700 pc region we briefly describe what could have happened since the probable close encounter of M 82 with M 81. Cottrell (1977) interpreted the observed large-scale kinematics of the neutral hydrogen gas in terms of tidal disruption of this gas from M 81 during the passage of M 82 on a hyperbolic orbit. The fact that the kinematic axis of the HI surrounding M 82 lies parallel to the major axis was seen as evidence for the captured gas to be in a polar orbit around M 82. In this picture, gas would eventually fall into the centre of M 82 and thus feed the starburst of this presumably former gas-poor galaxy.

Recently, Yun et al. (1994) have proposed the opposite scenario: the large HI streamers which they have found are interpreted as gas torn out of the outer gas-rich HI disk of M 82. The question arises how in this case gas is transported to the centre to feed the starburst. There is of course no contradiction because the tidal forces that are responsible for gas disruption in the outer disk of M 82 will also have caused instabilities in the gas orbiting in its inner part. It is well known that tidal interactions induce the rapid formation of bars along which gas can then be transported to the central regions of the galaxies. In view of this, the hypothesis of Yun et al. seems more attractive, because in this scenario gas may be transported more efficiently to the centre of M 82 than from a polar orbit. We therefore investigate in the following whether the observed kinematics of the ^{13}CO emission is consistent with this view.

The maps tracing the molecular gas in M 82 have been mostly interpreted in terms of a rotating molecular torus (e.g. Nakai et al. 1987; Loiseau et al. 1988; Shen & Lo 1995). As pointed out in Sect. 3.2, the ^{13}CO high resolution maps reveal a patchy gas distribution and a disturbed kinematics characteristic of gas in orbit around a stellar bar. The bar forces the outer gas to flow towards the central region, where it is exposed to the intense radiation field produced by the starburst and becomes largely dissociated. This is when the denser and better shielded clouds get shaped into the two lobes and the central condensation of Fig. 3.

We have compared several p-v diagrammes and find that they support this picture. These are: ^{13}CO (Fig. 6), [NeII] (Achtermann & Lacy 1995; their Fig. 4), H166α (Roelfsema & Goss 1992), H41α (Seaquist et al. 1996; their Fig. 5c), HCO$^+$ (Seaquist et al. 1996; their Fig. 5), and HCN (Brouillet & Schilke 1993; their Fig. 5; Shen & Lo 1995; their Fig. 4). From this we summarize the following: The brightest [NeII] emission peaks (concentrated between $\Delta\alpha{+}6''$ and $-11''$ around -110 km s^{-1}, see Fig. 9) coincide with depressions in ^{13}CO. The same holds true for the radio recombination lines, which shows that the effect does not just result from visual extinction variations. Finally, HCO$^+$(1$\rightarrow$0) closely follows the ^{13}CO emission and HCN(1$\rightarrow$0) is brighter near the nucleus and shows little evidence of a hole 7″ W of it.

The velocity-integrated emission maps of these lines show that the tracers of current star formation and the ionized gas are confined to radii of $\leq 10'' \ldots 14''$, which is also seen in the 3-mm continuum (free-free radiation) and the mid-infrared, the latter reflecting the heating of dust by young stars (Telesco & Gezari 1992). In contrast, the bulk of the CO gas is located beyond $\sim 10''$. The gas traced by the HCN molecule resides in very dense clouds that are better shielded against the radiation field.

6. Summary and conclusions

We have performed high-resolution observations of M 82 in the ^{13}CO(1$\rightarrow$0) line using the Plateau de Bure interferometer. The distribution and kinematics of this molecular species have been derived and analyzed, and a first comparison is made with existing interferometric data in the lines of ^{12}CO(1$\rightarrow$0) and HCN(1$\rightarrow$0).

The complex kinematic structure unveiled in previous studies is confirmed. Together with the asymmetric morphology of the observed distribution of the molecular gas it makes it difficult to maintain the hypothesis of an edge-on molecular torus, an idea advanced when the first low-resolution single-dish maps of the CO gas in the centre of M 82 became available. We rather propose that what we observe is the signature of a bar, the central (projected) 200 pc portion of which is relatively void of CO gas and probably subject to strong dissociation.

A 130 pc-wide emission hole is seen in our ^{13}CO data cube; it coincides with a region of enhanced high-J lines, recombination lines emission peak, and strong free-free and CI emission. It also hosts the young SNR 41.9+58. We think that this CO hole reflects a bubble inside which the gas is ionized and the molecules dissociated.

Maps of several transitions of the rare CO isotopomers would be needed to better constrain the cloud properties. Together with one arcsec resolution maps of CO and HCN, which could be directly compared to the optical pictures, they could yield a real understanding of how is triggered and fueld the most spectacular starburst in the vicinity of the Galaxy.

Acknowledgements. It is a pleasure to thank Drs. J. Shen and K.Y. Lo for making available to us their ^{12}CO(1-0) data from BIMA. We are very grateful to the referee, Dr. D. Jaffe, for his many helpful suggestions. UK is very indebted to IRAM for the warm hospitality and financial support.

References

Achtermann J.M., Lacy J.H., 1995, ApJ 439, 163
Brouillet N., Schilke P., 1993, A&A 177, 381
Carlstrom J.E., Kronberg P.P., 1991, ApJ 366, 422
Cottrell G.A., 1977, MNRAS 178, 577
García-Burillo S., Guélin M., Cernicharo J., 1993, A&A 274, 123
García-Burillo S., Guélin M., 1995, A&A 299, 657
García-Burillo S., Sempere M.J., Combes F., Neri R., 1998, A&A, 333, 864
Götz M., McKeith C.D., Downes D., Greve A., 1990, A&A 240, 52
Güsten R., Serabyn E., Kasemann C., et al., 1993, ApJ 402, 537
Henkel C., Bally J., 1985, A&A 150, L25
Joy M., Lester D.F., Harvey P.M., 1987, ApJ 319, 314
Jura M., Hobbs R.W., Maran S.P., 1978, AJ 83, 153
Klein U., Wielebinski R., Morsi H.W., 1988, A&A 190, 41
Kronberg P.P., Biermann P., Schwab F. 1985, ApJ 291, 693
Kuijken K., Merrifield M.R., 1995, ApJL, 443, L13
Larkin J.E., Graham J.R., Matthews K., et al., 1994, ApJ 420, 159
Lester D.F., Carr J.S., Gaffney N., Joy M., 1990, ApJ 352, 544
Lo K.Y., Cheung K.W., Masson C.R., et al., 1987, ApJ 312, 574
Loiseau N., Reuter H.-P., Wielebinski R., Klein U. 1988, A&A 200, L1
Loiseau N., Nakai N., Sofue Y., et al., 1990, A&A 228, 331
Nakai N., Hayashi M., Handa T., Sofue Y., Hasegawa T., 1987, PASJ 39, 685
Olofsson H., Rydbeck G., 1984, A&A 136, 17
Reynaud D., Downes D., 1997, A&A 337, 671
Rieke G.H., Loken K., Rieke M.J., Tamblyn P., 1993, ApJ 412, 99
Roelfsema P.R., Goss W.M., 1992, ARA&A 4, 161
Seaquist E.R., Bell M.B., Bignell R.C., 1985, ApJ 294, 546
Seaquist E.R., Carlstrom J.E., Bryant P.M., Bell M.B., 1996, ApJ 465, 691
Shen J., Lo K.Y., 1995, ApJ 445, L99
Smith P.A., Brand P.W.J.L., Puxley P.J., Mountain C.M., Nakai N., 1990, MNRAS 243, 97
Telesco C.M., Gezari D.Y., 1992, ApJ 395, 461
Telesco C.M., Harper D.A., 1980, ApJ 235, 392
White G.J., Ellison B., Claude S., Dent W.R.F., Matheson D.N., 1994, A&A 284, L23
Wild W., Harris A.I., Eckart A., et al., 1992, A&A 265, 447
Wilkinson P.N., de Bruyn A.G., 1990, MNRAS 242, 529
Wills K.A., Pedlar A., Muxlow T.W.B., Wilkinson P.N., 1997, MNRAS 291, 517
Yun M.S., Ho P.T.P., Lo K.Y., 1994, Nature 372, 530